III International Conference on Particle-based Methods – Fundamentals and Applications
PARTICLES 2013
M. Bischoff, E. Oñate, D.R.J. Owen, E. Ramm & P. Wriggers (Eds)

INVESTIGATIONS OF MICRO-STRUCTURE EVOLUTION IN GRANULAR SHEAR ZONES USING DEM

M. NITKA[1], J. TEJCHMAN[2] AND J. KOZICKI[3]

[1]Gdańsk University of Technology
80-233 Gdańsk-Wrzeszcz, Narutowicza 11/12
micnitka@pg.gda.pl

[2]Gdańsk University of Technology
80-233 Gdańsk-Wrzeszcz, Narutowicza 11/12
tejchmk@pg.gda.pl

[3]Gdańsk University of Technology
80-233 Gdańsk-Wrzeszcz, Narutowicza 11/12
jkozicki@pg.gda.pl

Key words: DEM, Earth Pressure, Granular Materials, Shear Zone, Vortex.

Abstract. The evolution of shear zones in initially medium dense cohesionless sand for quasi-static earth pressure problems of a retaining wall was analysed with a 3D discrete element method DEM using spheres with contact moments. The passive sand failure for a very rough retaining wall undergoing horizontal translation was discussed. Attention was laid on some micro-structural events appearing in shear zones (force chains, vortex structures, local density fluctuations). The calculated geometry of shear zones was compared with experimental results of laboratory model tests and finite element calculations.

1 INTRODUCTION

Earth pressure on retaining walls is one of the soil mechanics classical problems. In spite of an intense theoretical and experimental research over more than 200 years, there are still large discrepancies between theoretical solutions and experimental results due to the complexity of the deformation field in granular bodies near the wall caused by a spontaneous emergence of shear localization in the form of single or multiple narrow zones, which is a fundamental phenomenon of granular material behaviour at large shear deformation [1,2].

For granular materials, once a shear zone is formed, further deformation is mostly accommodated by the material within a shear zone. The peak and post-peak response of the material is thus controlled by localized shear zones. It is necessary to understand the underlying nature of granular material behaviour within shear zones to fully characterize the softening and critical state material response at the macro-level. The knowledge of both the distribution of shear zones and distribution of shear and volumetric strains within shear zones are important to explain the mechanism of granular deformation. The multiple patterns of shear zones are not usually taken into account in engineering calculations.

The objective of the paper is a numerical investigation of a quasi-static evolution of deformation micro-structure within shear zone in initially medium dense cohesionless sand with the discrete element method DEM. The DEM calculations were carried out in passive earth pressure conditions in sand behind a rigid vertical wall, which was moved towards the backfill. The three-dimensional spherical discrete model was used, allowing for introducing grain rolling resistance in order to take into account the grain roughness. Particle breakage was not considered because of the relatively low pressure level assumed in the simulations. Several characteristic micro-structural events occurring in shear zones at the grain-level such as force chains, vortex structures, local void ratio fluctuations and strain non-uniformities were analyzed.

2 DISCRETE ELEMENT METHOD

To simulate the behaviour of sand, a three-dimensional spherical discrete model YADE was developed at University of Grenoble [3] by taking advantage of the so-called soft-particle approach (i.e. the model allows for particle deformation which is modelled as an overlap of particles). To maintain the numerical stability of the method and to obtain a quick convergence to a quasi-static state of equilibrium of the assembly of particles, damping forces were introduced. In the paper, spherical elements were used only. To simulate sand grain roughness, additional moments were introduced into a 3D model, which were transferred through contacts and resisted particle rotations [3]. In this way, grains were in contact with their neighbours through a certain contact surface. Our discrete element model can simulate different grain shapes by using different symmetric and non-symmetric clusters of spheres [4]. In our computational model we used exclusively spherical particles and we modelled the influence of contact flatness and thus the effect of the grain shape by assuming bending moments and bending stiffnesses at particle contacts. In our approach, the computation time was significantly shortened (calculations with spheres and contact moments are 3-5 times faster than those using complex clumps [4]).

The interaction force vector $\vec{F}$ representing the action between two spherical discrete elements in contact was decomposed into a normal and tangential vector, respectively. A linear elastic contact model was assumed. The normal and tangential forces were linked to the displacements through the normal stiffness K_n and the tangential stiffness K_s (Figs.1a and 1b)

$$\vec{F}_n = K_n U \vec{N} \tag{1}$$

$$\vec{F}_s = \vec{F}_s + K_s \Delta \vec{X}_s \tag{2}$$

where U is the penetration depth between elements, $\vec{N}$ denotes the normal vector at the contact point and $\Delta \vec{X}_s$ is the incremental tangential displacement. The stiffness parameters were calculated with the aid of the modulus of elasticity of the grain contact E_c and two neighbouring grain radii R_A and R_B (to determine the normal stiffness K_n) and with the aid of the modulus of elasticity E_c and Poisson's ratio ν_c of the grain contact and two neighbouring grain radii R_A and R_B (to determine the tangential stiffness K_s), respectively [5]

$$K_n = E_c \frac{2R_A R_B}{R_A + R_B} \quad \text{and} \quad K_s = \nu_c E_c \frac{2R_A R_B}{R_A + R_B} \quad . \tag{3}$$

If the grain radius R_A=R_B=R, the stiffness parameters were equal to: K_n=E_c R and K_s=ν_c E_c R, respectively (thus K_s/K_n=ν_c). The frictional sliding started at the contact point if the contact forces $\vec{F}_s$ and $\vec{F}_n$ satisfied the frictional Mohr-Coulomb equation (Fig.1a)

$$\left\|\vec{F}_s\right\| - \left\|\vec{F}_n\right\| \times tan\mu \le 0\,, \tag{4}$$

where μ denotes the inter-particle friction angle. No forces were transmitted when grains were separated (tension was not allowed). The unloading was purely elastic. The elastic contact constants were specified from the experimental data of a triaxial compression test and could be related to the modulus of elasticity of grain material E and its Poisson ratio ν. A choice of a very simple linear elastic normal contact (Fig.1b) was intended to capture in average various contact possibilities possible in real sand.

In order to increase the rolling resistance of pure spheres, contact moments were introduced [3]. The normal force contributed to the rolling resistance only. The contact moment increments were calculated by means of the rolling stiffness K_r (Fig.1B)

$$\Delta M = K_r \Delta\vec{\omega} \quad \text{with} \quad K_r = \beta K_s R_A R_B \quad , \tag{5}$$

where β is the dimensionless rolling stiffness coefficient and $\Delta\vec{\omega}$ is the angular increment rotation between two spheres. In turn, the dimensionless rolling coefficient η controls the limit of the rolling behaviour

$$\left\|\vec{M}\right\| - \eta \frac{R_A + R_B}{2} \left\|\vec{F}_n\right\| \le 0. \tag{6}$$

To dissipate excessive kinetic energy in the discrete system, a simple local non-viscous damping scheme was adopted [6], which assumed a change of forces and moment by using the damping parameter α

$$\vec{F}^k_{damped} = \vec{F}^k - \alpha \cdot sgn(\vec{v}^k)\left|\vec{F}^k\right|, \qquad \vec{M}^k_{damped} = \vec{M}^k - \alpha \cdot sgn(\vec{\omega}^k)\left|\vec{M}^k\right|, \tag{7}$$

where $\vec{F}^k$ and $\vec{M}^k$ are the k^{th} components of the residual force and moment vector and $\vec{v}^k$ and $\vec{\omega}^k$ are the k^{th} components of the translational and rotational velocity [5]. A positive damping coefficient α is smaller than 1 (sgn(•) returns the sign of the k^{th} component of velocity). The equations can be separately applied to each k-th component of a 3D vector x, y and z. Note that the effect of damping is insignificant in quasi-static calculations. The following five main local material parameters are needed for discrete simulations: E_c, ν_c, μ, β and η. In addition, the particle radius R, particle density ρ and damping parameters α are required. The material strength increases with increasing μ, β and η.

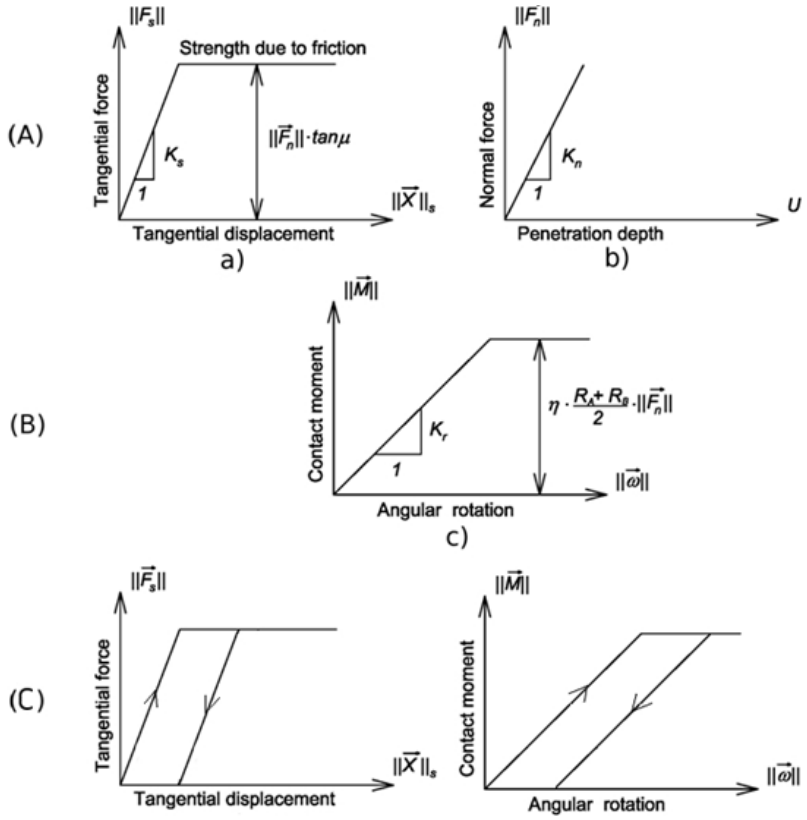

Figure 1: Mechanical response of linear contact model without (A) and with contact moments (A+B): a) tangential contact model, b) normal contact model and c) rolling contact model and C) loading and unloading path (tangential and rolling contact) [3], [5]

The material parameters were calibrated with axisymmetric triaxial laboratory test results on Karlsruhe sand by Wu [7]. The index properties of Karlsruhe sand are: mean grain diameter d_{50}=0.50 mm, grain size among 0.08 mm and 1.8 mm, uniformity coefficient U=2, maximum specific weight γ_d^{max}=17.4 kN/m^3, minimum void ratio e_{min}=0.53, minimum specific weight γ_d^{min}=14.6 kN/m^3 and maximum void ratio e_{max}=0.84. The sand grains are classified as sub-rounded/sub-angular. The triaxial compression laboratory tests were carried out with initially dense sand (initial void ratio e_o=0.53) and initially loose sand (e_o=0.80) in the confining pressure range σ_c=50-1000 MPa.

3. DISCRETE RESULTS OF EARTH PRESSURE PROBLEM

The discrete calculations were performed with a sand body of the length of 400 mm and height of 200 mm [2]. The height of the retaining wall was h=200 mm. The vertical retaining wall and the bottom of the granular specimen were assumed to be stiff and very rough, i.e. there were no relative displacements along a vertical and bottom surface. Since the effect of the specimen depth turned out to be almost negligible, discrete calculations were mainly performed with the specimen depth equal to the sphere size (i.e. only one grain layer was simulated in the perpendicular plane) in order to significantly accelerate simulations.

The calculations were carried out with three different mean grain diameters of spheres using a linear grain size range: d_{50}=5.0 mm (grain size range 2.5-7.5 mm, 2'600 spheres) d_{50}=2.0 mm (grain size range 1-3 mm, 15'600 spheres) and d_{50}=1.0 mm (grain size range 0.5-1.5 mm, 62'600 spheres). The initial void ratio of sand was e_o=0.625 obtained by generating spheres at random locations within a confined volume, applying gravity and waiting for their settlement. The loading speed was slow enough to ensure that tests were conducted under quasi-static conditions. The calculations were carried out with the parameters based on a triaxial compression test [7]: E_c=0.3 GPa, v_c=0.3, μ=18°, β=0.7, η=0.4, ρ=25.5 kN/m^3, a=0.08 with d_{50}=1 mm, 2 mm or 5 mm. The computation time CPU was ca. 14 days (d_{50}=2 mm) and 30 days (d_{50}=1 mm) using PC 3 GHz.

Figure 2 presents the calculated evolution of the resultant normalized horizontal earth pressure force $K=2E_h/(\gamma h^2 d_{50})$ versus normalized horizontal wall displacement u/h (h=0.2 m) by means of DEM for the different sphere size d_{50}=1-5 mm (E_h – the horizontal wall force). The normalized horizontal earth pressure force has a typical evolution for initially dense granulates during biaxial compression, triaxial compression and shearing. The specimen exhibits initial strain hardening up to the peak (u/h=0.03), followed by softening before reaching approximately an asymptote. It strongly fluctuates after the peak that is attributed to the build-up and collapse of force chains. For larger spheres, the parameter K_{max} becomes higher.

Figure 3 presents the typical particle configuration in the residual state (u/h=0.15) with the distribution of the sphere rotation ω. The red colour denotes the sphere rotation ω>+30° and the blue colour denotes the sphere rotation ω<-30°. The dark grey colour is related to the sphere rotation in the range $5^o \le \omega \le 30^o$ and the light grey to the range $-30^o \le \omega \le -5^o$ (the positive rotation (+) denotes the clockwise rotation). All grains in the range $-5^o \le \omega \le 5^o$ are in the medium grey colour. Shear zones can be clearly observed (only particles within shear zones significantly rotate). In turn, the distribution of the resultant sphere rotation ω^c and void ratio e is demonstrated in the granular specimen in Figs.4 and 5 and in the main curved shear zone in Fig.6. The quantities ω^c and e were calculated from the specimen area $5d_{50}\times 5d_{50}$ that was moved by (1-2) grains.

In general, the shear zones are clearly recognizable from the presence of the rotation ω and resultant rotations ω^c, shear deformation and an increase of void ratio e (Figs.3-6) First, the main curved shear zone forms at the bottom of the moving wall and propagates up to the top boundary (d_{50}=1-5 mm). Next, a radial shear zone appears at the wall top that propagates to the specimen bottom if d_{50}=1-2 mm. Except of the two main shear zones, there exist also in all 3 cases other less visible localized zones. The geometry with d_{50}=1-2 mm is similar as in experiments and in FE analyses [2]. The thickness t_s of the main curved shear zone increases with increasing mean grain diameter d_{50} (Fig.6). At the residual state, it is $t_s \approx 50$ mm ($10\times d_{50}$) with d_{50}=5 mm, $t_s \approx 33$ mm ($16\times d_{50}$) with d_{50}=2 mm and $t_s \approx 20$ mm ($20\times d_{50}$) with d_{50}=1.0 mm based on the distribution of grain rotation ω^c (Fig.6). It was assumed that shear localization takes place if $|\omega|>5^o$ (Fig.6a). The width grows in the range u/h=0.02-0.11.The mean inclination of a curved shear zone to the horizontal is 40° (d_{50}=1-5 mm) and is similar as in FE simulations [2]. In turn, the main radial shear zone is inclined to the vertical under 30° (d_{50}=2 mm) or 50° (d_{50}=1 mm) (in FE calculations: 35°-45° [2]). The maximum grain rotation ω in Fig.6 is about ω=75° at u/h=0.15.

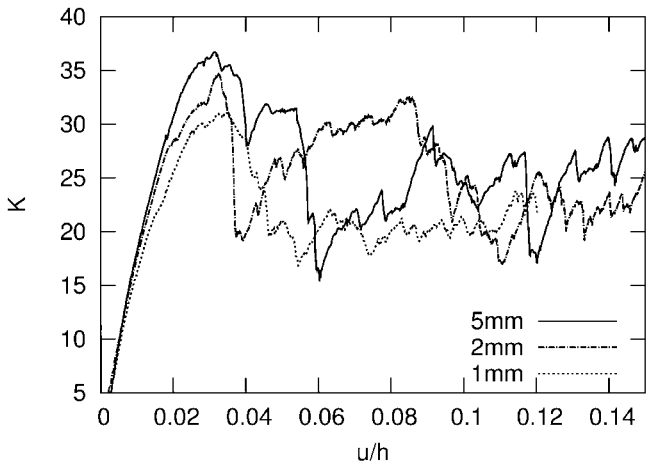

Figure 2: DEM results (passive case, translating wall): evolution of resultant normalized horizontal earth pressure force $2E_h/(\gamma h^2 d_{50})$ versus normalized horizontal wall displacement u/h for different mean grain diameter d_{50}=1-5 mm (γ=16.75 kN/m^3, h=0.2 m, e_o=0.63, d_{50}=1-5 mm)

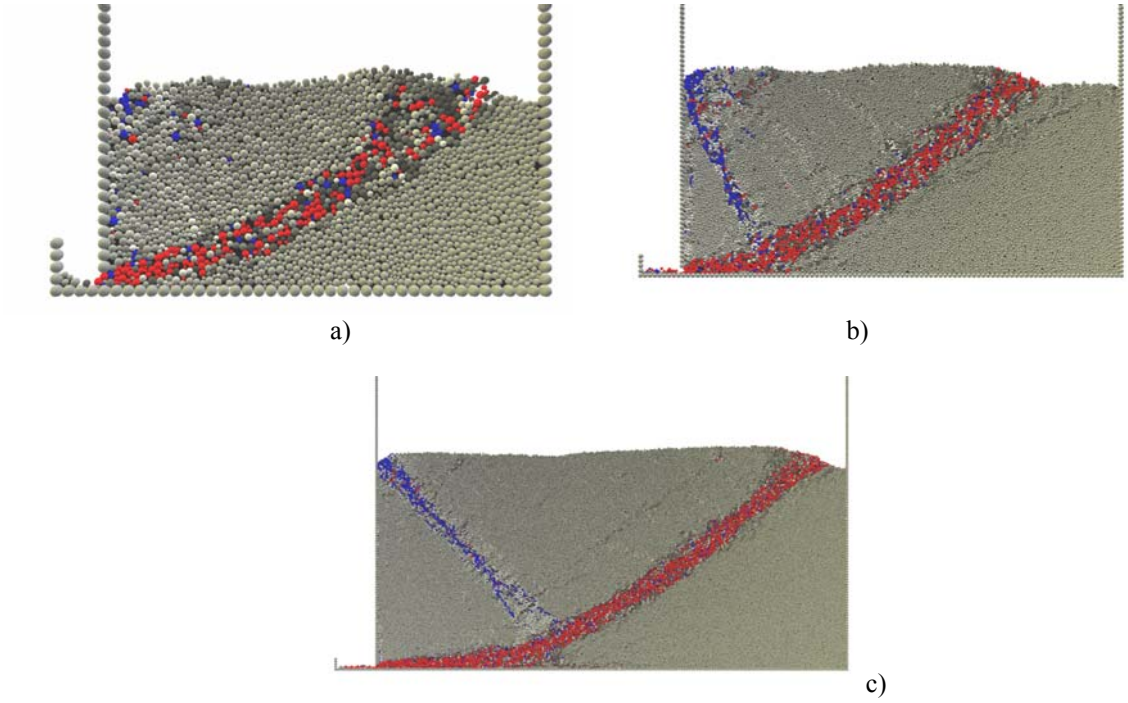

Figure 3: Deformed granular body 0.2×0.4 m^2 with distribution of rotation for initially medium dense sand (e_o=0.62) from DEM at residual state of u/h=0.15: a) d_{50}=5 mm, b) d_{50}=2 mm and c) d_{50}=1 mm (red colour denotes clockwise rotation ω>+30^o, blue colour denotes anticlockwise rotation ω<-30^o)

The distribution of the resultant grain rotations ω^c is non-uniform in the region between the wall and curved shear zone (Fig.3). It is non-uniform in the curved and radial shear zone along their length (Fig.4A) and width (Fig.6a). The resultant grain rotation ω^c has its maximum in the

mid-width of the shear zone. It is equal to 70° (d_{50}=1.0-2.0 mm) and 45° (d_{50}=5.0 mm) at u/h=0.15. At u/h=0.05 it is 35° (d_{50}=1.0 mm). A parabolic distribution of ω^c and e across a shear zone (Fig.6) is similar as in FE calculations [2]. The distribution of void ratio across the shear zone is also strongly non-uniform with its maximum value along the centreline (Figs.4 and 6). The void ratio alternates along a shear zone in a nearly periodic fashion (Fig.5) as in biaxial compression tests based on the DIC technique [8]. The specimen globally dilates in the shear zones, however, the local void ratio can also reduce. Thus, local contractancy in the shear zone is obtained (Fig.6c). The maximum value of e in the shear zone at the residual state is about 0.74 (Fig.6) and is similar as in FE calculations [2] (e=0.78). Beyond the shear zone, the void ratio is about e=0.63-0.65 (Fig.6).

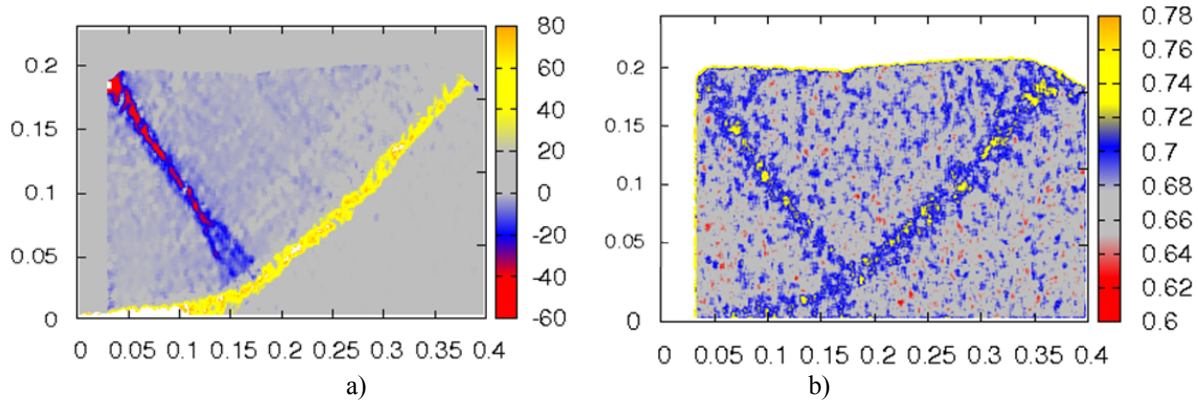

Figure 4: Distribution of resultant grain rotation ω^c (a) and void ratio (b) in initially medium dense sand (e_o=0.62, d_{50}=1 mm) from DEM at residual state of u/h=0.15
(scale denotes grain rotation intensity in [°], yellow colour (+) - clockwise rotation)

The evolution of the contact network in the granular specimen is demonstrated in Fig.7. The colour intensity represents the different compressive normal contact force between two particles (red colour – great normal contact forces, higher than average normal contacts, green colour – small normal contact forces, lower than average normal contacts). The distribution of internal contact forces is non-uniform and continuously changes. Force chains of heavily loaded grain contacts bear and transmit the compressive load on the entire granular system and are the predominant structure of internal forces at micro-scale. They build up and collapse. The force chains are created mainly in a region between the wall, radial and curved shear zone and along a curved shear zone. They are the highest at the wall (Fig.7A). Thus, the anisotropy of the numerical test is very strong due to obliquely oriented force chains. In a curved shear zone at the residual state, the strongest force chains are perpendicular to the shear zone line (Fig.7Bc).

The number of contacts diminished in a curved shear zone during wall translation due to sand dilatancy leading to a reduction of the stability of force chains (Fig.7B). At the deformation beginning, the total contact number in the granular specimen was equal to 119’154 (and for the small region of Fig.7B, the contact number was 10’090). When a shear zone was started to form, this number decreased down to 109’859 (8 946) at

u/h=0.045. At u/h=0.09 the contact numbers was 108'276 (8'538), and at u/h=0.15 was 107'777 (8'038).

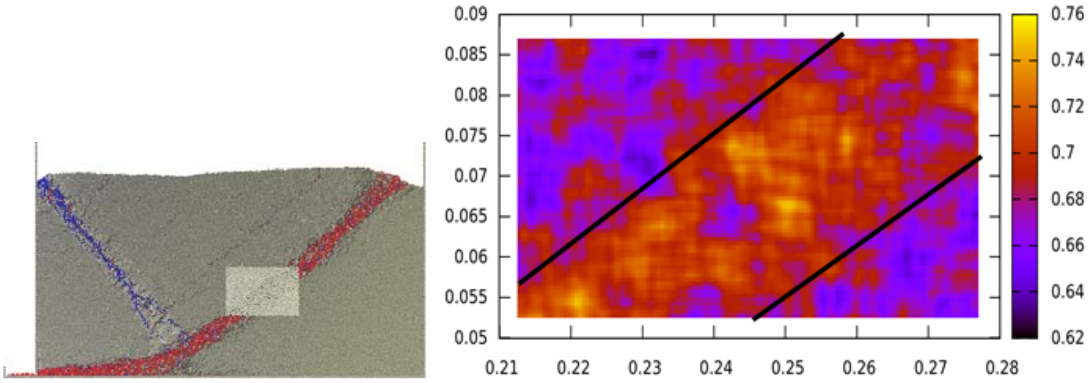

Figure 5: DEM results (e_o=0.625, d_{50}=1 mm): distribution of void ratio e in mid-region of curved shear zone in initially medium dense sand at horizontal wall displacement of u/h=0.15 (vertical left axis – vertical co-ordinate, vertical right axis - void ratio, horizontal axis – horizontal co-ordinate, solid lines - edges of shear zone)

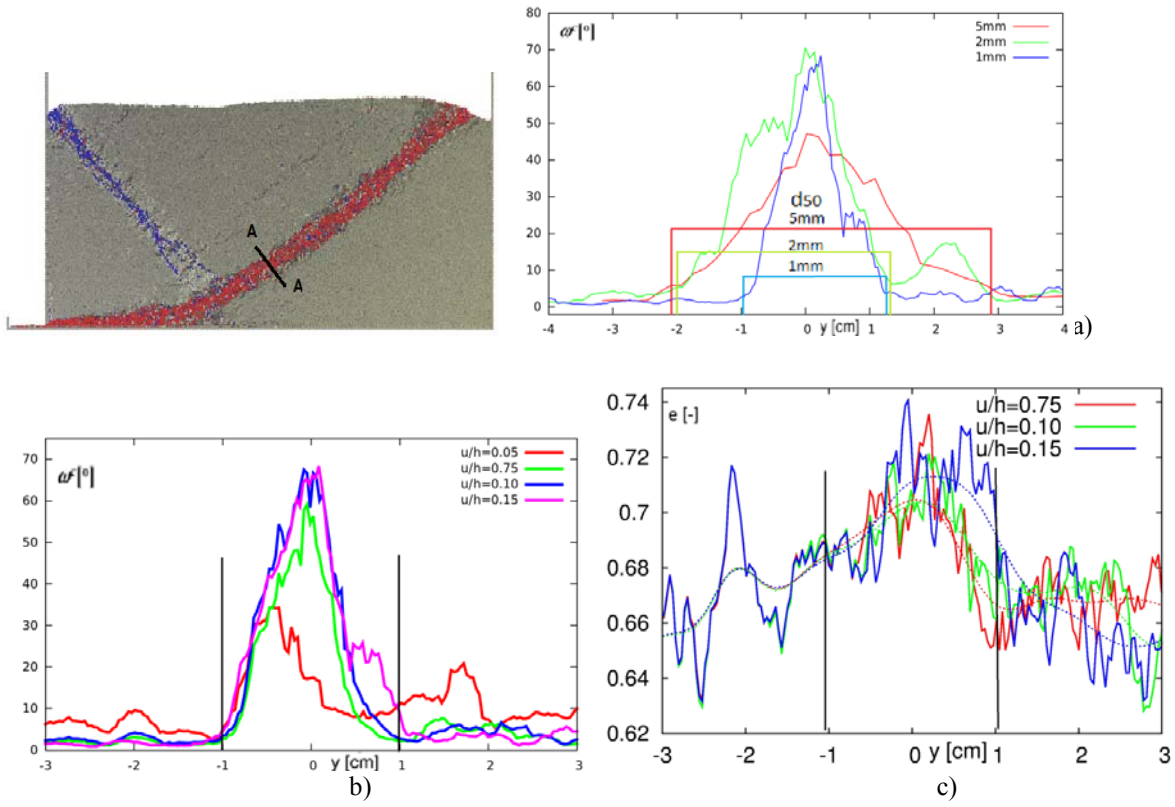

Figure 6: DEM results (initially medium dense sand, e_o=0.625): a) distribution of resultant grain rotation ω^c across curved shear zone width 'y' in initially medium dense sand at residual state of u/h=0.15 for different mean grain diameter d_{50}=1-5 mm, b) distribution of ω^c against u/h (d_{50}=1 mm) and c) distribution of void ratio e against u/h (d_{50}=1 mm) (dotted line in 'b' corresponds to average values) (vertical solid line – edges of shear zone)

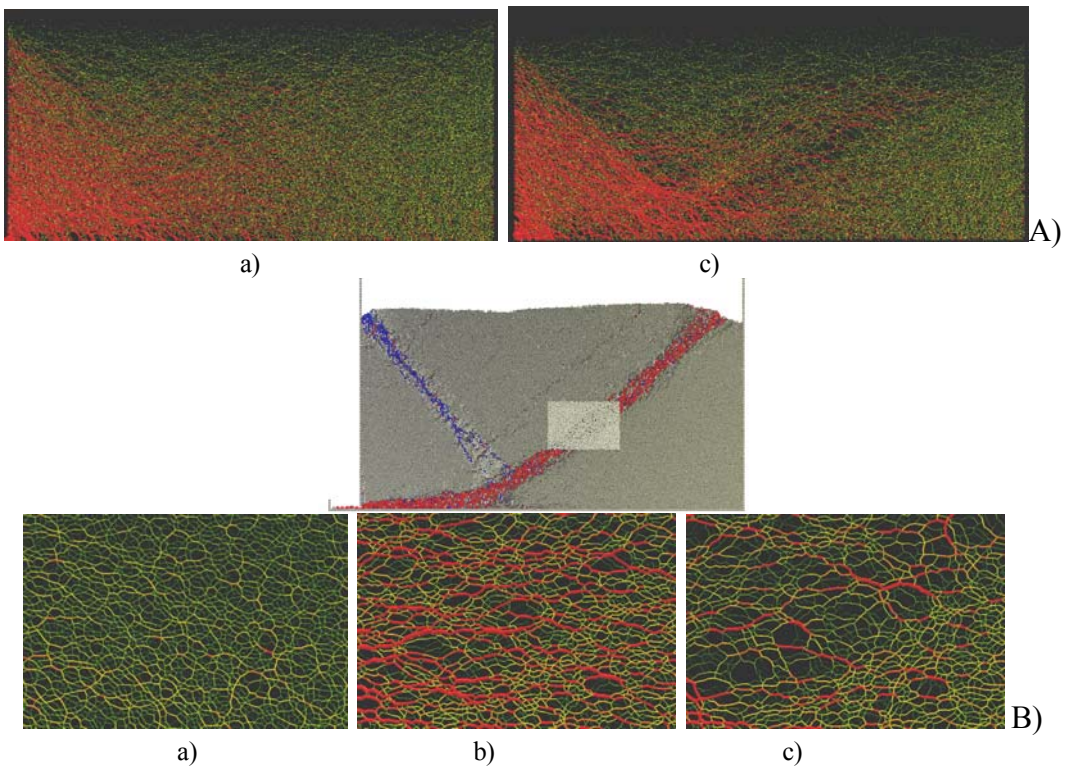

Figure 7: Distribution of contact normal forces between spheres (e_o=0.62, d_{50}=1 mm) from DEM at: a) u/h=0.02 (without shear zone) b) u/h=0.06 (shear zone appearance), c) u/h=0.15 (full development of shear zone): A) entire granular specimen, B) zoom on mid-region of curved shear zone

Figure 8 presents a spontaneous occurrence of displacement fluctuations in the shear zone in the form of clusters of circulating cells (so-called vortex structures) observed both in quasi-static experiments [9,10] and discrete simulations [11,12]. It is hypothesized that this non-uniform micro-structure is related to buckling of force chains. The plots were obtained by drawing the displacement difference vector ($\vec{V}_i - \vec{V}_{avg}$) for each sphere with respect to the background translation corresponding to the homogeneous (affine) strain ($\vec{V}_i$ represents the sphere displacements during e.g. 100 iterations and $\vec{V}_{avg} = \frac{1}{n}\sum_i^n \vec{V}_i$ are the average displacements). The individual particle displacements are able to form large long-range deformation vortex structures, wherein cells rotate as a rigid body whereas the space between them is characterized by intense shear deformation. The vortex-like patterns are well recognized in particular at the residual state with the highest mean grain diameter d_{50}=5 mm (Fig.8). Several vortices (3 at d_{50}=5 mm and 10 at d_{50}=1 mm) occur along a curved shear zone with the diameter of about t_s. They rotate anticlockwise. The distance between vortexes is variable – some of them are close to each other (at the distance of about t_s) or far away from each other (at the distance of about $5\times t_s$).

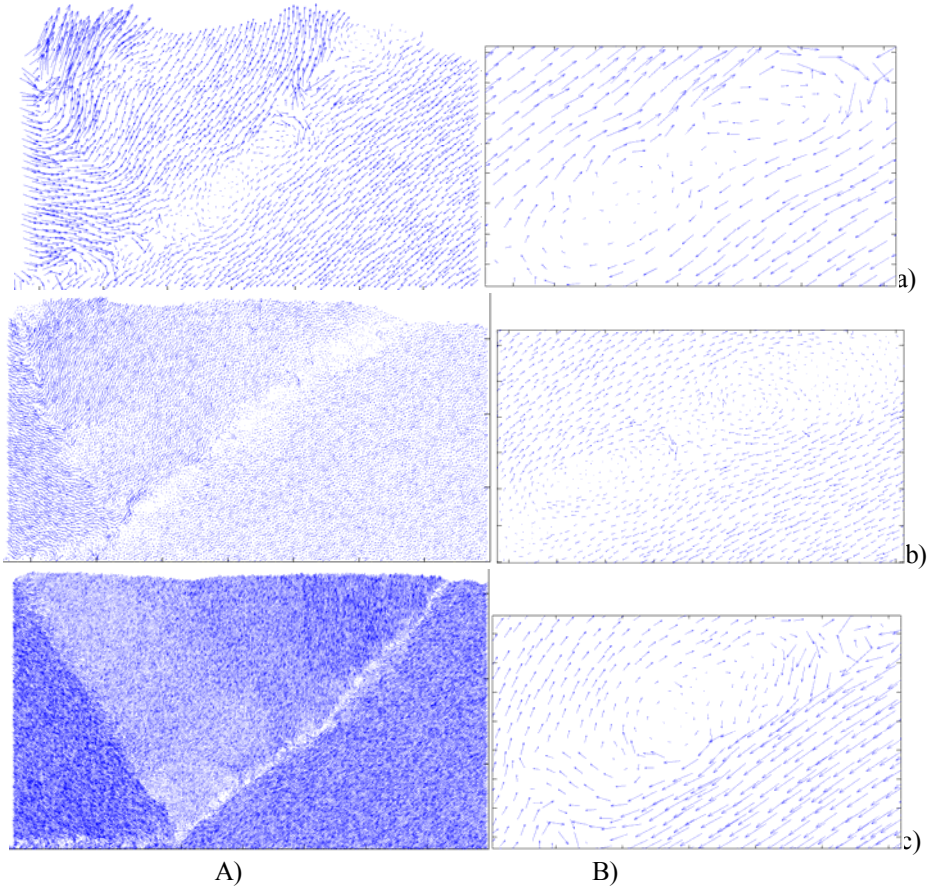

Figure 8: DEM results: formation of displacement fluctuations in form of vortex structures in curved shear zone at residual state of u/h=0.15: a) d_{50}=5 mm, b) d_{50}=2 mm and c) d_{50}=1.0 mm, A) entire granular specimen, B) zoom on mid-region of curved shear zone

A link between force chain, vortex structure and void ratio changes in the region 70×100 mm^2 of a curved shear zone at the residual state during wall normalized displacement interval of u/h=0.01 (from u/h=0.15 up to u/h=0.16) is described in Fig.9 with d_{50}=5 mm.

A vortex structure exists at u/h=0.15 (Fig.9Aa) and is not visible at u/h=0.16 (Fig.9Ba). In turn, a force chain vanishes at u/h=0.15 (Fig.9Ba) and a new force chain occurs at u/h=0.16 (Fig.9Bb). Small dilatancy occurs close to a broken force chain (Figs.9Ac-9Ae) and small contractancy happens near a new force chain (Figs.9Bc and 9Bd). Thus, the occurrence and vanishing of vortex structures strictly corresponds to force chain changes.

4. CONCLUSIONS

- DEM realistically predicts the experimental results of a pattern of shear zones in the interior of initially medium dense sand behind a retaining wall. The global wall pressure increases with increasing mean grain size. Grain rotations are noticeable only in shear zones. Dilatancy takes place in shear zones with small local contractancy regions.

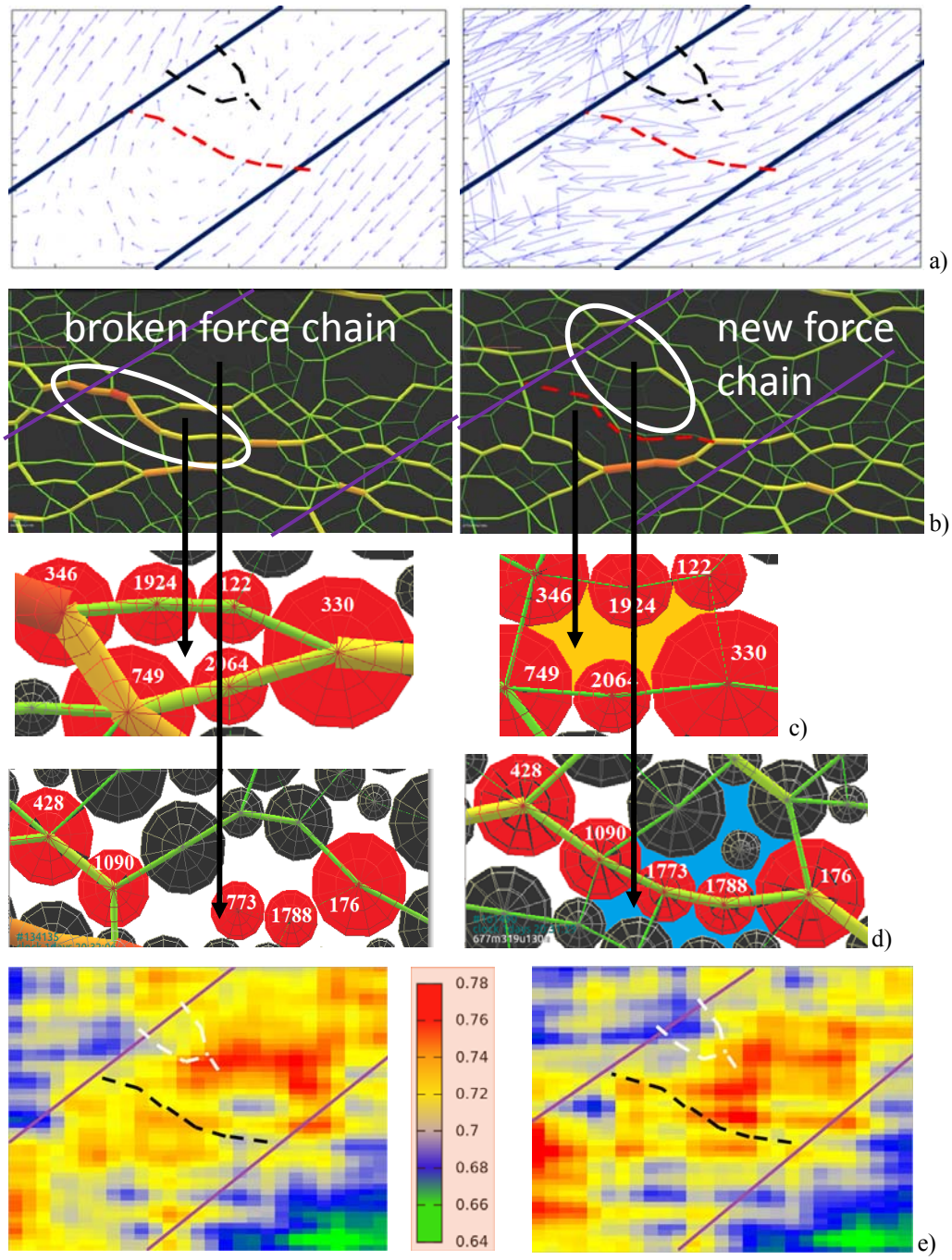

Figure 9: DEM results (e_o=0.62, d_{50}=5 mm): evolution of micro-structures in curved shear zone for normalized wall displacement interval of u/h=0.01 at u/h=0.15 (A) and u/h=0.16 (B): (solid lines- shear zone edges) a) map of displacement fluctuations of Fig.15Ba (red dashed line – broken force chain, black dashed line – new force chain), b) geometry of force chains between spheres (red dashed line – broken force chain), c) and d) zoom on geometry of force chains and spheres (red spheres are in force chain, yellow colour between spheres denotes higher void ratio, blue colour between spheres denotes lower void ratio), d) map of void ratio with intensity scale (red colour corresponds to higher void ratio, black dotted line - broken force chain, white dotted line - new force chain)

- In shear zones, vortex structures and local void ratio fluctuations systematically occur that seem to have a periodically organized structure. The number of vortices increases with decreasing mean grain diameter. The distance between vortices increases with increasing mean grain diameter. The vortices are a direct manifestation of grain rearrangement.
- The distribution of internal contact forces is non-uniform due to a build-up and collapse of force chains. The number of contact forces continuously decreases in a granular specimen due to material dilatancy.
- The deformation of force chains plays a key role in the formation of vortex structures. The collapse and build-up of force chains is connected with vanishing and appearing vortices, respectively. The collapse of force chains leads also to a formation of larger voids and their build-up to a formation of smaller voids.

REFERENCES

[1] Gudehus, G. and Nübel, K. Evolution of shear bands in sand. *Geotechnique* (2004) 113, **54** (3):187–201.

[2] Tejchman, J. *FE modeling of shear localization in granular bodies with micro-polar hypoplasticity*. Springer Series in Geomechanics and Geoengineering (eds. Wu and Borja), Springer Verlag, Berlin-Heidelberg, (2008).

[3] Kozicki, J. and Donze, F.V. A new open-source software developed for numerical simulations using discrete modelling methods. *Computer Methods in Applied Mechanics and Engineering* (2008) **197**:4429-4443.

[4] Kozicki, J., Tejchman, J. and Mróz, Z. Effect of grain roughness on strength, volume changes, elastic and dissipated energies during quasi-static homogeneous triaxial compression using DEM. *Granular Matter* (2012) **14** (4):457-468.

[5] Šmilauer, V. and Chareyre, B. *Yade DEM Formulation*. Manual, (2011).

[6] Cundall, P.A. and Hart, R. Numerical modeling of discontinua. *J. Eng. Comp*. (1992) **9**:101-113.

[7] Wu, W. Hypoplastizität als mathematisches Modell zum mechanischen Verhalten granularer Stoffe. *Heft 129, Institute for Soil- and Rock-Mechanics, University of Karlsruhe,* (1992).

[8] Chupin, O, Rechenmacher, A.L and Abedi, S. Finite strain analysis of non-uniform deformations inside shear bands in sands. *International Journal for Numerical and Analytical Methods in Geomechanics* (2012) **36**(14):1651-1666.

[9] Abedi, S., Rechenmacher, A.L. and Orlando, A.D. Vortex formation and dissolution in sheared sands. *Granular Matter* (2012) **14** (6):695-705.

[10] Richefeu, V., Combe, G. and Viggiani, G. An experimental assessment of displacement fluctuations in a 2D granular material subjected to shear. *Geotechnique Letters* (2012) **2**: 113–118.

[11] Kuhn, M.R. Structured deformation in granular materials. *Mechanics of Materials* (1999), **31**: 407-442.

[12] Liu, X., Papon, A. and Mühlhaus, H.-B. Numerical study of structural evolution in shear band. *Philosophical Magazine* (2012), doi.org/10.1080/14786435.2012.715249.